Journal of Cell Science 113, 291-302 (2000)
Printed in Great Britain © The Company of Biologists Limited 2000
JCS0958

The path of RNA through nuclear pores: apparent entry from the sides into specialized pores

Francisco J. Iborra, Dean A. Jackson and Peter R. Cook*

Sir William Dunn School of Pathology, University of Oxford, South Parks Road, Oxford OX1 3RE, UK
*Author for correspondence (e-mail: peter.cook@path.ox.ac.uk)

Accepted 9 November 1999; published on WWW 13 January 2000

SUMMARY

The path that RNA takes through nuclear pores was mapped using two high-resolution techniques. Unexpectedly, no RNA in HL60 cells was detected by immunogold labelling in the central axis of the pore complex on its way to the transporter at the nuclear membrane; instead, it was distributed around the sides, apparently entering just before the membrane. In rat liver nuclei, poly(A)$^+$ RNA, hnRNPs A1 and C, mrnp 41, ASF, and a phosphorylated subset of SR proteins were also distributed like mRNA, as were various transport factors and their cargoes (NTF2, Ran, RCC1, karyopherin β, Rch1, transportin α, m^{2,2,7}-trimethylG). Many pores were associated with particular transport factors/cargoes to the exclusion of others; some were associated with poly(A)$^+$ RNA or phosphorylated SR proteins (but not NTF2), others with NTF2 (but not poly(A)$^+$ RNA or the SR proteins). Electron spectroscopic imaging confirmed these results. Some pores contained phosphorus-rich RNA apparently entering from the sides; others lacked any phosphorus, and were surrounded by a ribosome-free zone in the cytoplasm. The results also suggest that pores have different functional zones where SR proteins are dephosphorylated, and where hnRNP C is removed from messages.

Key words: Bromouridine, Electron spectroscopic imaging, Immunogold labelling, Nuclear pore, Nuclear transport

INTRODUCTION

The nuclear pore acts as a gate in the nuclear envelope that permits exchange of macromolecules between nucleus and cytoplasm (reviewed by Akey, 1995; Bastos et al., 1995; Davis, 1995; Panté and Aebi, 1996; Mattaj and Englmeier, 1998; Yang et al., 1998). It is a huge wheel-like assembly (>1 MDa) of multiple copies of >100 different proteins arranged with eightfold symmetry. A central transporter is connected through eight spokes to two coaxial rings; eight thin fibres also project from one ring into the cytoplasm, while a basket projects from the other into the nucleus (Jarnik and Aebi, 1991; Goldberg and Allen, 1992; Akey and Radermacher, 1993).

Macromolecules are transported in both directions through pores. Protein import has been studied extensively, mainly using biochemical and genetic approaches. It involves three main phases, docking at the outer fibres, translocation through the central channel, and substrate release (reviewed by Nigg, 1997; Ullman et al., 1997; Mattaj and Englmeier, 1998). Docking involves recognition of specific nuclear localization sequences (NLSs) by specific receptors (e.g. basic NLSs by importin-β/karyopherin-β1, the M9 sequence by transportin/karyopherin-β2), and translocation requires GTP hydrolysis catalyzed by Ran/TC4 GTPase (reviewed by Koepp and Silver, 1996). RNA export also involves recognition of specific RNA motifs by special receptors (e.g. transportin/karyopherin β), requires energy, and may utilize Ran GTPase (Nakielny et al., 1997). It has been studied using various approaches (Mattaj and Englmeier, 1998). One involves direct observation of dense RNPs in the electron microscope; for example, mRNP particles have been seen passing through the central channel (Stevens and Swift, 1966; Franke and Scheer, 1974). Export of 50 nm particles containing the 75S RNA encoded by the BR genes of *Chironomus* has been particularly intensively studied (reviewed by Daneholt, 1997; Kiseleva et al., 1998). It is thought that this large particle docks at the tip of the basket which projects into the nuclear interior, and then unfolds so that the 5′ end of the transcript associated with the cap binding complex can lead the way through the centre of the basket to the transporter embedded in the coaxial rings. Another approach involves microinjecting gold particles coated with RNA into the nucleus, and following their passage through the pore (Dworetzky and Feldherr, 1988; Feldherr and Akin, 1997; Panté et al., 1997). In situ hybridization also shows poly(A)$^+$ RNA to be concentrated along the central axis of the pore (Huang et al., 1994). In yet another approach, cells are grown in Br-U, which is incorporated by RNA polymerases into RNA; the resulting Br-RNA can be detected by immunogold labelling on its way through the pore to the cytoplasm (Iborra et al., 1998). Analogous approaches have been used to analyze protein import (e.g. Dworetzky and Feldherr, 1988; Görlich et al., 1996; Panté and Aebi, 1996; Panté et al., 1997).

We have now applied the two highest resolution techniques

available, immunogold labelling and electron spectroscopic imaging, to map the paths that natural cargoes takes through pores; unextracted cells were used to minimize the formation of artifacts. Unexpectedly, we found no cargoes or transport factors in the middle of basket; instead, they were all distributed around the edges, apparently entering or leaving from the sides close to the transporter. We also found several distinct populations of pore. For example, some pores were associated only with poly(A)$^+$ RNA and others only with NTF2. This raises the possibility that at any one moment certain pores specialize in export, others in import.

MATERIALS AND METHODS

Cell growth

HL60 cells were grown in RPMI plus 10% bovine calf serum (both from GibcoBRL, Paisley, UK) and 2.5 mM Br-U. This concentration of Br-U had essentially no effect on the incorporation of [2-^{3}H]adenosine (5 μCi/ml; 20 Ci/mmol; Amersham Pharmacia Biotech, Herts, UK) into acid-insoluble material over 0.5 and 1 hour, incorporation being 102 and 92% of that of controls incubated without the analogue (not shown).

Antibodies

The following mouse monoclonal antibodies were used: anti-nucleoporin p62 (used at 5 μg/ml; Transduction Laboratories, Lexington, KY), anti-NUP153 (clone QE5; IgGκ; used at 10 μg/ml; Berkeley antibody company; Berkeley, California), antibody 414 (used at 1 in 2,500; IgGκ; Berkeley antibody company), anti-Tpr (used at 5 μg/ml; clone 203-37; IgG1; Oncogene Research Products, Cambridge, MA), anti-NTF2 (IgG; used at 5 μg/ml; Transduction Laboratories), anti-Ran/TC4 (used at 5 μg/ml; IgG2a; Transduction Laboratories), anti-RCC1 (used at 2.5 μg/ml; Transduction laboratories), anti-karyopherin β (used at 5 μg/ml; IgG1; Transduction Laboratories), anti-Rch1 (used at 5 μg/ml; Transduction Laboratories), transportin (used at 5 μg/ml; clone 23; mouse IgG1; Transduction Laboratories), anti-hnRNP A1 (1:1000; a gift from G. Dreyfuss; Piñol$^-$Roma and Dreyfuss, 1992), anti-hnRNP C (used at 1 in 500; a gift from G. Dreyfuss; Piñol-Roma and Dreyfuss, 1992), anti-SR (IgM; 1 in 100 dilution of culture supernatant of clone 104; ATCC CRL-2067; Roth et al., 1990), anti-ASF (used at 1 in 250; a gift from A. Krainer; Cáceres et al., 1998), anti-mrnp 41 (used at 1 in 500; a gift from G. Blobel; Kraemer and Blobel, 1997), and anti-m^{2,2,7}G (used at 1:200 dilution; Calbiochem, Nottingham, UK).

In situ hybridization

Poly(A) was detected by in situ hybridization (Visa et al., 1993). Grids with Lowicryl sections were floated on drops of hybridization solution containing 20 μg/ml biotin-(dT)50 (Genosys, Cambridge, UK), hybridized (37°C; 4 hour) in a wet chamber, washed five times in PBS at room temperature, and non-specific binding blocked by incubation (>30 minutes) in PBBT. Bound biotin was detected using a primary mouse anti-biotin (5 μg/ml; Jackson Immunoresearch Laboratories, PA) and a secondary goat anti-mouse IgG conjugated with 10 nm gold particles (1:25 dilution; British Biocell International, Cardiff, UK). After washing with PBS, sections were fixed (1% glutaraldehyde; 15 minutes), washed with water and air dried. Specificity of labelling was verified by pretreating (1 hour; 37°C) sections with RNase A (1 mg/ml; Boehringer Mannheim, Sussex, UK) in 10 mM Tris-HCl (pH 7.3) before hybridization; this reduced labelling to background levels (see below).

Immunogold labelling and electron microscopy

HL60 cells were prefixed (10 minutes; 0°C) with 4% paraformaldehyde in 250 mM Hepes (pH 7.4), fixed (50 minutes; 20°C) with 8% paraformaldehyde in the same buffer, partially dehydrated in ice-cold ethanol, embedded in LR White (polymerization by heat for 4 hour at 50°C; London Resin Company, Berks, UK). Livers were extracted from Wistar rats, fixed (60 minutes; 4°C) with 0.5% glutaraldehyde and 4% formaldehyde (both from TAAB Laboratory Equipment Ltd, Reading, UK) in 100 mM sodium cacodylate buffer (pH 7.4; Merck, Darmstadt, Germany), incubated (60 minutes) in 50 mM NH_4Cl, and embedded in Lowicryl K4M (Agar Scientific, Essex, UK), as described by Renau-Piqueras et al. (1989). For Fig. 2A, samples were transferred after fixation to 1% OsO_4 plus 1.5% ferrocyanide, washed, embedded in Epon (Agar Scientific), sectioned, and stained with uranyl acetate and lead citrate.

Ultrathin sections (50 nm) on nickel grids were indirectly immunolabelled on one surface only using IgGs conjugated with 5 or 10 nm gold particles. When labelling one protein antigen, nonspecific binding was blocked by preincubation (30 minutes) in PBBT. PBBT is PBS (pH 8.2) with 1% BSA and 0.1% Tween-20. Then, sections were incubated (2 hour) with primary antibodies diluted in PBBT, washed in PBS (pH 8.2), incubated (1 hour) with a secondary goat anti-mouse IgG absorbed on to gold particles (1:25 dilution in PBBT, spun immediately before use to remove aggregates; British Biocell International), rewashed, and fixed with 2.5% glutaraldehyde. Next, sections were washed with water, dried, contrasted with a saturated solution of uranyl acetate in 70% ethanol, and digital images collected using a Zeiss 912 Omega electron microscope (Iborra et al., 1996).

Other antigens were detected as above with the following modifications. Br-RNA was detected using a primary monoclonal anti-bromodeoxyuridine antibody (10 μg/ml in PBS with Tween and BSA; Boehringer Mannheim) that reacts with Br-RNA, a secondary rabbit anti-mouse IgG (1:50 dilution; Jackson Immunoresearch Laboratories), and a tertiary goat anti-rabbit IgG absorbed on to 10 nm gold particles (1:25 dilution spun as above; British Biocell International). SR and NTF2 were detected together using the two primary antibodies (an IgM and IgG, respectively), then a mixture of goat anti-IgM conjugated with 10 nm particles (as above) and a rabbit anti-mouse Fc fragment (1 in 100 dilution; Organon Teknika NV, Turnhout, Belgium), and finally with goat anti-rabbit IgG conjugated with 5 nm particles (1 in 25 dilution; British Biocell International). Poly(A) and NTF2 were detected together by incubating sections which had been hybridized with biotin-(dT)50 (as above) first with the anti-NTF2, and then with a mixture of the goat anti-biotin IgG conjugated with 5 nm particles (1 in 100 dilution; British Biocell International) and a goat anti-mouse IgG conjugated with 10 nm particles (as above).

Quantitative analysis after immunogold labelling

Images were analyzed using 'Esivision' software (Soft-imaging Software GmbH, Münster, Germany). Pores were recognized as gaps of 100-140 nm in the layer of peripheral heterochromatin surrounding nuclei. A system of coordinates was obtained by drawing one straight line over the outermost edge of the heterochromatin across a pore, and another perpendicular to the first through the middle. Coordinates of each gold particle were collected and exported to Microsoft 'Excel', where distributions were analyzed. Background labelling was not subtracted, as it was so low. Thus, when detecting proteins antigens, controls incubated without primary antibodies gave 1 particle in 520 'small', 160 'medium', and 125 'large' fields (defined in Table 1). When detecting poly(A), RNase-treated controls (see above) gave 1 particle in 545 'small' fields, 180 'medium' fields, and 110 'large' fields.

As many immunolabelling particles lay over the edge of heterochromatin close to pores, we were concerned that this might reflect non-specific binding. Therefore, we counted particle numbers over eu- and hetero-chromatin at different distances from the inner nuclear membrane into the interior. Generously, we considered a particle to lie over heterochromatin if it lay up to 30 nm

Table 1. Numbers of labelled pores (determined using images like Fig. 4)

	Number pores analyzed	Pores with label in field (%)			Number particles in all +ve fields
		'Large' 	'Medium' 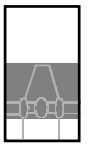	'Small' 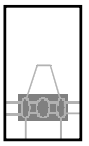	'Small' 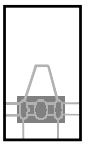
Single-labelling					
1. poly(A)	532	7	4	3	42
2. NTF2	210	40	39	34	287
3. SR	306	34	24	11	222
Double-labelling, poly(A) + NTF2					
4. poly(A) alone	880	5	4	3	74
5. NTF2 alone	880	37	37	33	1,115
6. poly(A) and NTF2	880	2	0.1*	0.1*	1 poly(A), 2 NTF2
7. poly(A) and NTF2 (calculated)		3	1	1	19 poly(A), 27 NTF2
Double-labelling, SR + NTF2					
8. SR alone	306‡	21	25	10	216
9. NTF2 alone	306‡	30	40	34	403
10. SR and NTF2	306‡	10	0*	0*	0 SR, 0 NTF2
11. SR and NTF2 (calculated)		13	10	4	31 SR, 36 NTF2
Double-labelling, poly(A) + SR					
12. poly(A) alone	654	nd	4	nd	
13. SR alone	654	nd	154	nd	
14. poly(A) and SR	654	nd	18§	nd	
15. poly(A) and SR (calculated)	654	nd	5	nd	

A pore was considered labelled if it contained ⩾1 particle in a grey field. Backgrounds (see Materials and Methods) were not subtracted. In rows 7 and 11, values were calculated from products of frequencies (%), and that frequency, the number of pores analyzed, and the number of particles per pore (number particles).

*Probability >0.998 that the one marker excludes the other from the area tested (determined using chi-squared test).

‡Only 108 pores analyzed for 'large' field.

§Probability >0.999 that one marker did not exclude the other from the test area.

nd: not done.

from heterochromatin. 94, 98, 54 and 17% particles marking phosphorylated SR antigens were found over heterochromatin between 0-20, 21-100, 101-200, and 201-300 nm from the membrane (not shown). Corresponding figures for particles marking poly(A)$^+$ RNA were 89, 88, 29, and 17% (not shown). These results show that these SR antigens and poly(A)$^+$ RNA were specifically concentrated over heterochromatin close to pores, but not further away; therefore, this concentration cannot be due to non-specific binding to the edge of heterochromatin.

Electron spectroscopic imaging (ESI)

Hendzel and Bazett-Jones (1996) and Hendzel et al. (1998) describe the application of ESI to estimate phosphorus content. Livers were fixed as above, transferred to 1% OsO_4 plus 1.5% ferrocyanide, washed, embedded in Epon, and sections (40 nm) collected on nickel grids. Using 'EasiVision' software supplied with the Zeiss 912 Omega electron microscope, four images of each region were collected (i.e. at zero energy loss at 80 kV, and at −112, −120, and −155 eV with slit-widths of 15 eV); each image contained 512×512 pixels of 4.2 nm^2. Then, background in the −155 eV window was estimated (using the '3 window exponential method') and subtracted to give the net phosphorus image.

Intensities in net phosphorus images were calibrated by reference to cytoplasmic ribosomes, assuming each contained 6,600 phosphorus atoms uniformly spread through a sphere (Hendzel et al., 1998). In Fig. 7A-D, ribosomes have variable diameters and intensities because some lie on top of others in the ~40 nm section, others are cut randomly during sectioning, while a few remain as 'polar caps' with so little mass or phosphorus that they go undetected. The most frequent class had the diameter (i.e. ~20 nm) expected of an intact ribosome, and so was assumed to contain 6,600 phosphorus atoms (Fig. 7E); other intensities (arbitrary units determined from the average grey level × pixel number) could then be scaled directly to number of atoms. This calibration was confirmed by comparison with a reference distribution obtained by simulation using a 'Windows' program called 'Nucleus' written by Matthew Lloyd. This program simulates the appearance of a section of a nucleus containing randomly-distributed (red and green) spheres; the program cuts off the top and bottom of a sphere if the boundary of the slice intersects a sphere. Pixel size, sphere number and diameter, degree of sphere blurring, section thickness, and size of nucleus can all be specified. The distribution of sphere size and volume (intensity) measured in simulated images matched the distribution found with ribosomes (Fig. 7E). The threshold of detection was determined (Fig. 7, legend), and all net phosphorus images show intensities above this threshold.

Average phosphorus distributions around pores were determined using Adobe 'Photoshop' and linked sets of images like those in Fig. 8A-D. Pores with gaps of >100 nm in the membrane were selected using the −120 eV image, the shortest lines drawn across the gap, and image sets aligned in a stack (using the coordinate system shown in Fig. 8E). Next, the average intensity of each pixel in the stack of net phosphorus images was calculated (Fig. 8F). Then, 'phosphorus$^+$ pores' and 'phosphorus$^-$ pores' were selected (using the net phosphorus image in each set) and the difference image obtained by subtraction. As pores are symmetric about the central axis and cut randomly, the average intensity of each pixel in the resulting image, and of each pixel in the mirror image, is presented in Fig. 8I.

RESULTS

Br-RNA in transit through HL60 pores detected by immunolabelling

When HeLa cells are grown in Br-U, the analogue is incorporated into RNA and exported to the cytoplasm. As polymerase I incorporates Br-U poorly and rRNA contains so few U residues, the bromine is mainly found in mRNA. This Br-RNA can be detected by immunogold labelling and electron microscopy with great sensitivity, because each can contain many tens of epitopes (i.e. bromines), and not the one commonly found in a protein antigen (Iborra et al., 1998). Immunogold detection involves compromises that affect labelling efficiency and structural visualization (Griffiths, 1993); here, we generally maximize labelling efficiency. However, this means that it is sometimes difficult to identify unambiguously pores in HeLa cells that have little peripheral heterochromatin. Therefore, we used HL60 cells (a human myeloid line) in which pores are easily identified. The cells were grown for different periods in Br-U, fixed, sectioned (~50 nm), embedded, and any Br-RNA on one surface of the section immunolabelled. Then, pores appear as gaps in peripheral heterochromatin. In order to maximize resolution, only gaps of 100-140 nm in the peripheral heterochromatin (i.e. pores sectioned at or close to the equator) were chosen for analysis. As cells are grown in Br-U for longer, the intensity of immunogold labelling over nuclei increases (Fig. 1A,C), and soon gold particles were found over pores and the cytoplasm (Fig. 1E). Particles often abut the heterochromatin flanking the pore (Fig. 1E). This concentration was not due to non-specific binding to heterochromatin; it was only seen up to 100 nm away from the pore, even though heterochromatin was found further into the interior (see Materials and Methods).

For quantitative analysis, we counted the numbers and positions of all gold particles within a ‘large’ rectangle around 125 pores. Each rectangle extended 100 nm along the membrane to each side of the pore, 250 nm from the inner nuclear membrane into the nucleus, and 100 nm towards the cytoplasm. As structural details of the pore are not visible in such sections of unextracted material, a cartoon of the pore is placed in the appropriate position in the rectangle in the scatter plots presented below (Fig. 1B,D,F). This cartoon is derived mainly from studies of pores in nuclear envelopes isolated from *Xenopus* oocytes, as we so not know the precise dimensions of mammalian pores. It is included solely to provide a sense of context, and of scale in and around pores. Note that our criteria for selecting pores ensures that all are sectioned equatorially at the level of the membrane, but more remote regions (e.g. the tip of any basket) may be lost from some sections if the pore happens to be appropriately oriented. However, a study of many pores should in theory enable distributions around these remote regions to be established (albeit with less precision), and we show that in practice proteins in such regions can be detected (see below). The resulting plots give the impression that as the concentration of Br-RNA increases, more Br-RNA passes around the edges of the basket to enter the pore from the side just above the inner membrane. No Br-RNA was detected on the expected path (i.e. down through the middle of the basket). (Background labelling can be neglected, as only 1 particle was seen in 125 rectangles; Materials and Methods.)

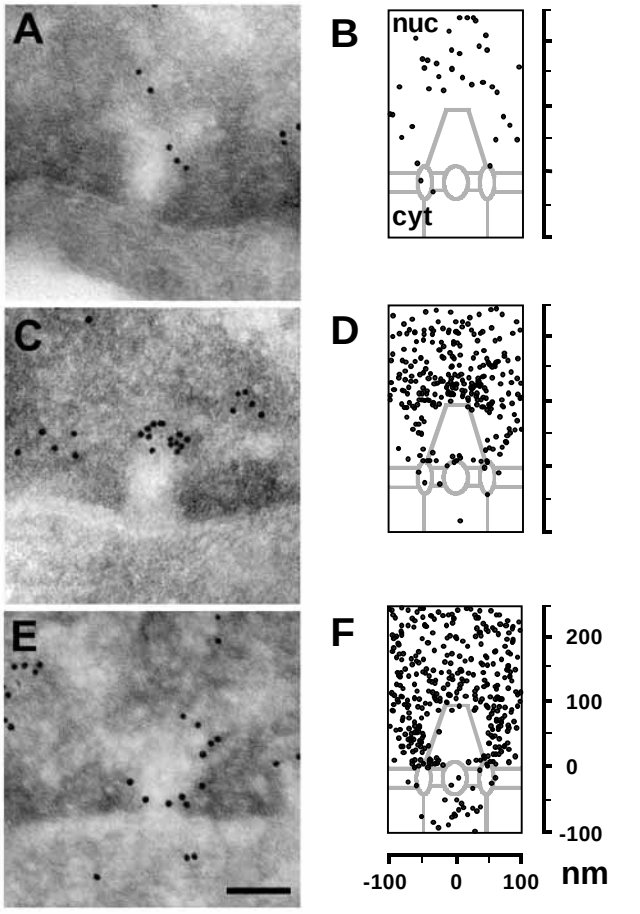

Fig. 1. Accumulation of Br-RNA at pores in HL60 cells. Cells were grown in 2.5 mM Br-U for various times, Br-RNA indirectly immunolabelled with gold particles (10 nm), images collected (representative electron micrographs are shown on the left), and the positions of all particles in a rectangle (200 × 350 nm) over the pore determined. The positions of all particles seen over 125 pores are indicated on the right, with a diagram (drawn at the same scale; bar, 100 nm) showing the relative positions of membrane bilayer and pore complex. In all images presented, nuclei are at the top. (A,B) After 10 minutes in Br-U, only a few particles are seen. (C,D) After 30 minutes, more particles are concentrated over the tip of the basket, and a few are found along the inner coaxial ring or between the cytoplasmic filaments. (E,F) After 60 minutes, high concentrations are found over the nucleus (except the basket), and more are seen over the cytoplasm.

This distribution of Br-RNA resembles that of SV40 particles seen in infected nuclei (Maul, 1976).

Localizing proteins in and around pores in rat liver nuclei

We next analyzed the distribution of various proteins in and around pores in rat liver nuclei, chosen because their pores are even more easily recognized than those in HL60 cells. Thus, after a harsh fixation in glutaraldehyde and osmium, embedding in Epon, and staining with heavy metals, pores are easily seen (Fig. 2A). Despite the excellent ultrastructure, this procedure largely destroys antigenicity (Griffiths, 1993); therefore, cells were fixed more gently, embedded in Lowicryl, and immunolabelled as

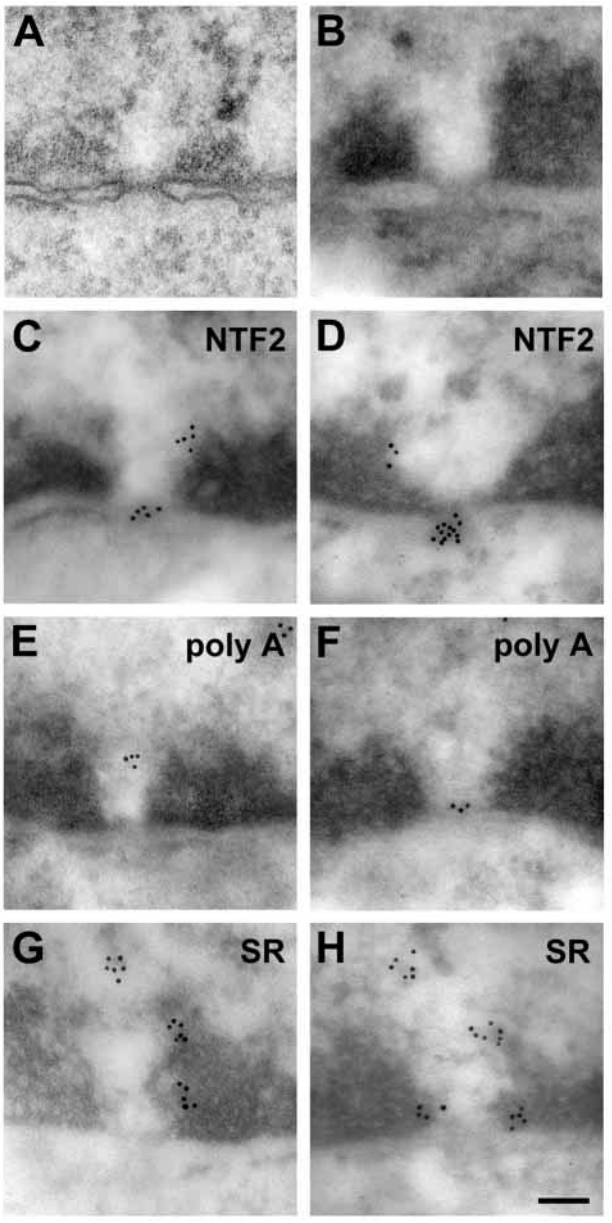

Fig. 2. Electron micrographs of nuclear pores in rat liver cells (hepatoctyes). (A) Epon embedment. Membranes and peripheral heterochromatin are well stained, and the pore appears as a gap in the membrane. (B) Lowicryl embedment. Membranes are not stained, but pores are visible as gaps in peripheral heterochromatin. The white region at the bottom left probably represents an area originally containing an aggregate of glycogen granules. (C,D) Two images showing 10 nm particles marking NTF2, which is often seen in the gap in the membrane and close to heterochromatin. (E,F) Two images showing 10 nm particles marking poly(A)$^+$ RNA (obtained by in situ hybridization). (G,H) Two images showing 10 nm particles marking a phosphorylated subset of SR proteins. Bar, 100 nm.

before (Fig. 2B). Although membranes are now not so well defined and some glycogen granules in the cytoplasm are lost (Bozzola and Russell, 1992), pores can still be identified as gaps in the peripheral heterochromatin; they are found at the same density in Lowicryl sections as in Epon sections (i.e. 2±0.5 and 1.9±0.6 pores per μm of membrane, respectively; not shown). Moreover, glycogen loss had no effect on immunolabelling; pores near white cytoplasmic regions (which probably originally contained an aggregate of glycogen granules) were immunolabelled much like others (not shown). Importantly, most antigens analyzed could be detected with higher efficiencies; representative examples are illustrated in Fig. 2C-H, and scatter plots illustrating the distributions are shown in Fig. 3.

Components of the pore complex all gave the expected labelling pattern. Nucleoporin (NUP) p62, part of the transporter (Davis and Blobel, 1986), was only found at the level of the membrane in the centre of the complex (Fig. 3A), while antibody QE5, which recognizes p62 as well as NUPs 153 and 250 (Panté et al., 1994), labelled the central axis of the pore complex from basket tip, through the transporter, to the cytoplasm (Fig. 3B). Monoclonal antibody 414 (Davis and Blobel, 1986) labelled the transporter and basket tip (Fig. 3C), while Tpr, a filamentous protein attached to the nuclear side and which is involved in mRNA export (Cordes et al., 1997; Bangs et al., 1998), was dispersed around the basket (Fig. 3D).

Various factors facilitate transport through the pore (reviewed by Nigg, 1997; Ullman et al., 1997; Mattaj and Englmeier, 1998), including NTF2 (Fig. 3E; Moore and Blobel, 1994; Paschal and Gerace, 1995; Smith et al., 1998), Ran (Fig. 3F; Melchior et al., 1993), RCC1 (Fig. 3G; Moore and Blobel, 1994; Paschal and Gerace, 1995), karyopherin β/importin β (Fig. 3H; Rexach and Blobel, 1995), the armadillo-repeat protein Rch1 (Fig. 3I; Moroianu et al., 1995), and transportin (Fig. 3J; Pollard et al., 1996). None were found in the middle of the basket, and both RCC1 and karyopherin β were confined to the nucleus.

A number of markers tested travel with mRNA, and so would be expected to have the same distribution as Br-RNA in HL60 cells (Fig. 3R). Indeed, poly(A)$^+$ RNA (Figs 2E,F, 3K), hnRNP A1 (Fig. 3L; Nakielny and Dreyfuss, 1997), and hnRNP C (Fig. 3M; Piñol-Roma and Dreyfuss, 1992) were distributed much like Br-RNA, although hnRNP C travelled only as far as the pore (Fig. 3M). SR proteins are a group of splicing factors that contain serine- and arginine-rich carboxy-terminal domains; most are unphosphorylated and found in large 'speckles' or interchromatin granule clusters in the nuclear interior (Zahler et al., 1992; reviewed by Kramer, 1996), but a phosphorylated subset accompanies RNA from primary transcription sites as far as pores (Figs 2G,H, 3N; Iborra et al., 1998). A specific SR protein, the splicing factor ASF/SF2 (Cáceres et al., 1998), is also found on the cytoplasmic side of the pore (Fig. 3O). As phosphorylated ASF/SF2 is detected by the antibody used to visualize phosphorylated SR proteins, this is consistent with ASF/SF2 being dephosphorylated just before it passes through the membrane. Mrnp 41, another protein that might accompany the message (Kraemer and Blobel, 1997), is also distributed much like Br-RNA (Fig. 3P). One marker tested probably travels only in the other direction. The snRNAs U1-U5 are transcribed by RNA polymerase II, capped with a m^7G, and exported to the cytoplasm; there, the cap is hypermethylated to $m^{2,2,7}$-trimethylG and, after association with Sm proteins, snRNP particles return to the nucleus, where they probably remain (Görlich and Mattaj, 1996). Trimethyl caps are seen in the cytoplasm, central transporter and around the basket (Fig. 3Q). Again, none of these markers were found in the middle of the basket.

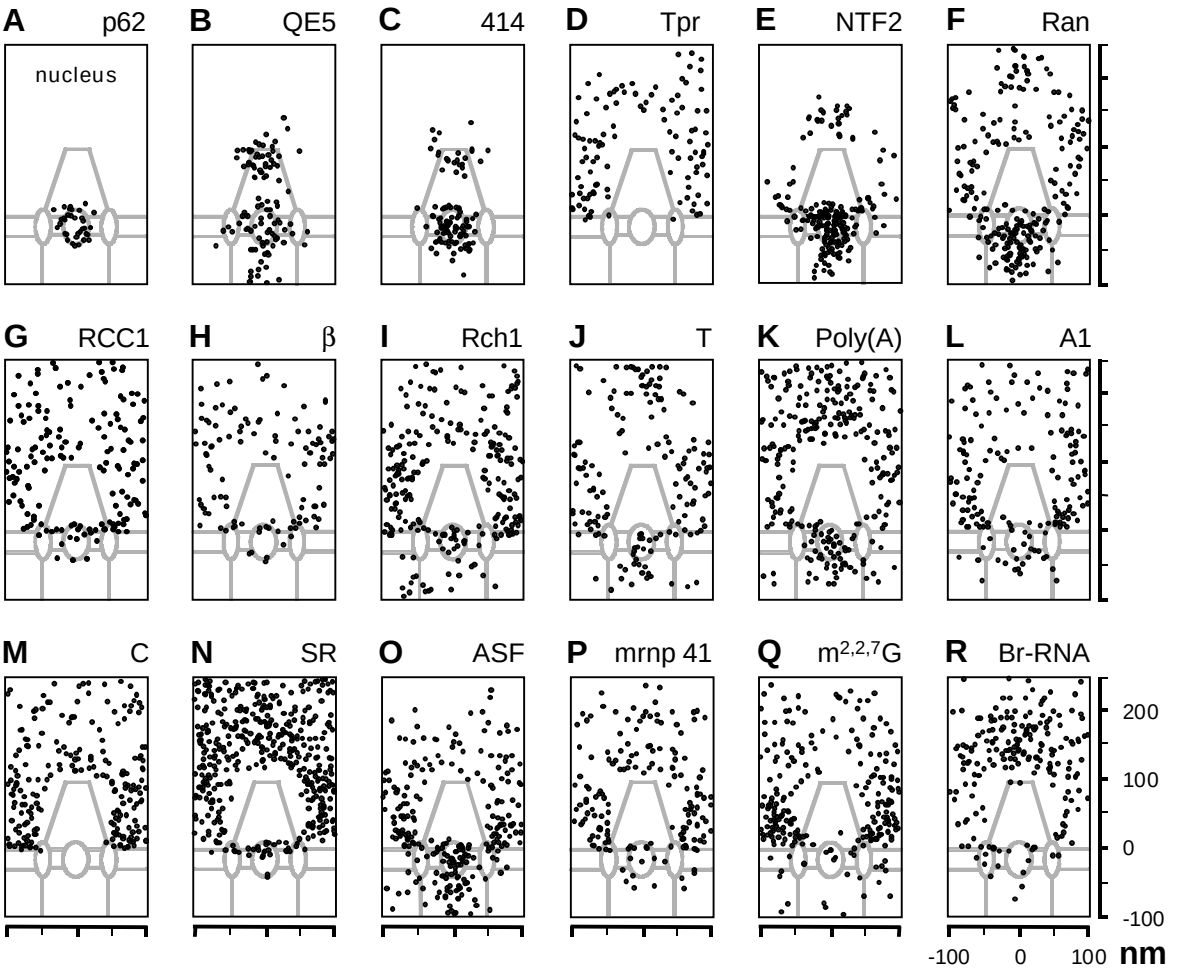

Fig. 3. The distributions of different markers around pores of rat liver nuclei. Scatter plots for each marker were obtained as in Figs 1 and 2. Background levels were 0.008 particles/field (determined by omission of primary antibody). The distribution of Br-RNA (1 hour labelling) in HL60 cells is included in (R) for completeness.

Categorizing different types of pore

We next used double immunolabelling to examine whether a particular pore was associated with one specific cargo/factor to the exclusion of another. Whether a cargo/factor is imported or exported does not affect this analysis; our concern is whether a pore is associated with one, or both, markers. After labelling poly(A)$^+$ RNA and NTF2, we found only one doubly-labelled pore amongst 880 analyzed; this is the frequency of background labelling (see below). With this one exception, pores that appeared to have poly(A)$^+$ RNA (marked by small particles) in transit across the membrane were not associated with NTF2 (marked by large particles; Fig. 4A), and pores with NTF2 at the membrane were not associated with poly(A)$^+$ RNA (Fig. 4B).

For quantitative analysis, we categorized pores as associated either with poly(A) or with NTF2 using an approach that is exemplified by reference to single-labelling experiments. Under our conditions, 7% pores have ≥1 particle marking poly(A)$^+$ RNA within the field analyzed (see below), and their particle distribution is illustrated in Fig. 5A,1. However, many particles might mark mRNA not yet associated with a pore. Therefore, we selected the subset of pores that had ≥1 particle over the 'small' grey rectangle illustrated in Fig. 5A,2. We call these 'poly(A)$^+$ pores', since the marker is so closely associated with the gap in the membrane. As some of these pores are also associated with particles outside the grey rectangle, we obtain the distribution illustrated in Fig. 5A,3. 'SR$^+$ pores' and 'NTF2$^+$ pores' are defined similarly (Fig. 5B,C). SR is distributed around 'SR$^+$ pores' in a characteristic way (Fig. 5B,3; see below).

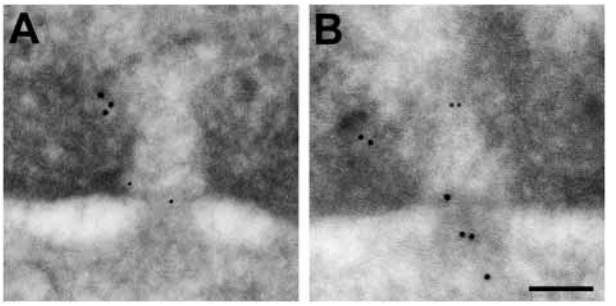

Fig. 4. (A,B) Pores in Lowicryl sections of rat liver nuclei after double-immunolabelling with 5 and 10 nm particles marking poly(A)$^+$ RNA and NTF2, respectively. Bar, 100 nm.

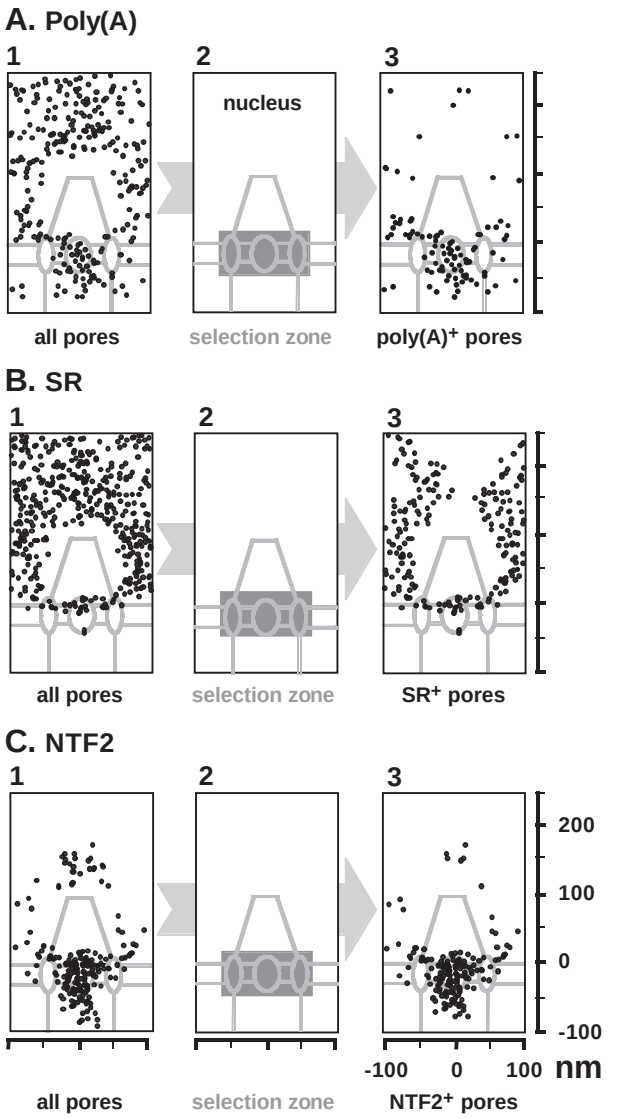

Fig. 5. Categorizing pores of different types. Scatter plots for poly(A), SR, and NTF2 shown in Fig. 3 are reproduced in column 1. Pores with particles lying within the grey rectangle illustrated in column 2 were selected, and the their distributions are shown in column 3. The selection zone extended 70 nm along the membrane to each side of the pore, 50 nm from the inner nuclear membrane towards the cytoplasm, and 20 nm into the nucleus. As immunolabelling particles can lie up to 20 nm away from the antigen they mark, this zone extends 20 nm in each direction away from gap of 100 × 30 nm in the membrane.

Some pores are associated with poly(A), others with NTF2

We next analyzed the distributions of particles marking poly(A)$^+$ RNA and NTF2 in 880 images like those illustrated in Fig. 4. Some pores contained ≥1 small particle (marking poly(A)$^+$ RNA) as well as ≥1 large particle (marking NTF2) within the 'large' field analyzed initially (e.g. those illustrated in Fig. 4); the distributions of poly(A) (Fig. 6A,1) and NTF2 (Fig. 6B,1) in this field were similar to those seen by single labelling (Fig. 5A,1 and Fig. 5C,1). Although considerable numbers of particles marking poly(A) were seen apparently passing through the gap in the membrane of 'poly(A)$^+$ pores' (Fig. 6A,2), only one, equivalent to background labelling, was found in the gap of 'NTF2$^+$ pores' (Fig. 6A,3). Conversely, only two particles marking NTF2, again equivalent to background labelling, were found near the gap in 'poly(A)$^+$ pores' (Fig. 6B,2) despite the high numbers found in 'NTF2$^+$ pores' (Fig. 6B,3). Clearly, NTF2 is excluded from the gap in 'poly(A)$^+$ pores', and vice versa. Moreover, the exclusion zone extends ~100 nm into the nucleus (Fig. 6A,3 and Fig. 6B,2), and so cannot be due to steric hindrance. In this double-labelling experiment, 56% pores apparently contained no poly(A)$^+$ RNA or NTF2; this could be due to inefficient labelling or the presence of a subset of pores lacking either factor (see Discussion).

Some pores are associated with a subset of SR antigens, others with NTF2

Poly(A)$^+$ RNA is detected inefficiently by our procedures (see below), so 880 pores had to be analyzed to obtain the above distributions (Table 1, lines 4-6). Therefore, we analyzed the phosphorylated subset of SR proteins that are detected more efficiently. Although these SR proteins play a role in splicing (Zahler et al., 1992; Kramer, 1996), they also seem to accompany messages from their site of synthesis as far as the pore (Iborra et al., 1998; Iborra and Cook, 1998). Like poly(A)$^+$ RNA, they are completely excluded from 'NTF2$^+$ pores' (Fig. 6C,3) despite their concentration at the membrane and up the sides of the basket of 'SR$^+$ pores' (Fig. 6C,2). Conversely, NTF2 is completely excluded from 'SR$^+$ pores' (Fig. 6D,2), despite its concentration in the gap of 'NTF2$^+$ pores' (Fig. 6D,3). Again, the exclusion zone extends ~100 nm into the nucleus. These results show that some pores associate with SR proteins to the exclusion of NTF2, and vice versa.

Quantitative analysis of immunogold labelling

Exclusion of poly(A) and SR proteins from the 'small' area around an 'NTF2$^+$ pore' was confirmed by quantitative analysis (Table 1). Thus, 0.1% pores (i.e. only 1) were seen that contained both poly(A) and NTF2 within this area, compared to the 1% (i.e. 8) expected if the two markers were distributed independently (compare lines 6 and 7). These 8 pores would be expected to contain 19 'poly(A) particles' and 27 'NTF2 particles', instead of the 1 and 2 actually observed (lines 7 and 6). Moreover, no pores were seen with both SR and NTF2 within the 'small' area, although 4% (i.e. 11) were expected (compare lines 10 and 11). Again, these 11 pores would be expected to contain 31 'SR particles' and 36 'NTF2 particles', rather than the none observed (lines 11 and 10). An analogous exclusion was seen in the grey area of 'medium' size (covering 100 nm on each side of the pore, 50 into the cytoplasm, and 100 nm into the nucleus); for example, no pores were seen with both SR and NTF2 (line 10), compared to the 10% expected (line 11).

Several reasons suggest that this exclusion is a property of individual pore complexes. First, the exclusion did not have some unforseen systematic basis, as it was not seen with the 'large' area (Table 1, compare lines 6 with 7, and 10 with 11). Second, it could not result from steric hindrance by one antibody complex of another, as the same percentages of pores were detected by single- and double-labelling. For example, 3% pores contained poly(A) in the 'small' area after single

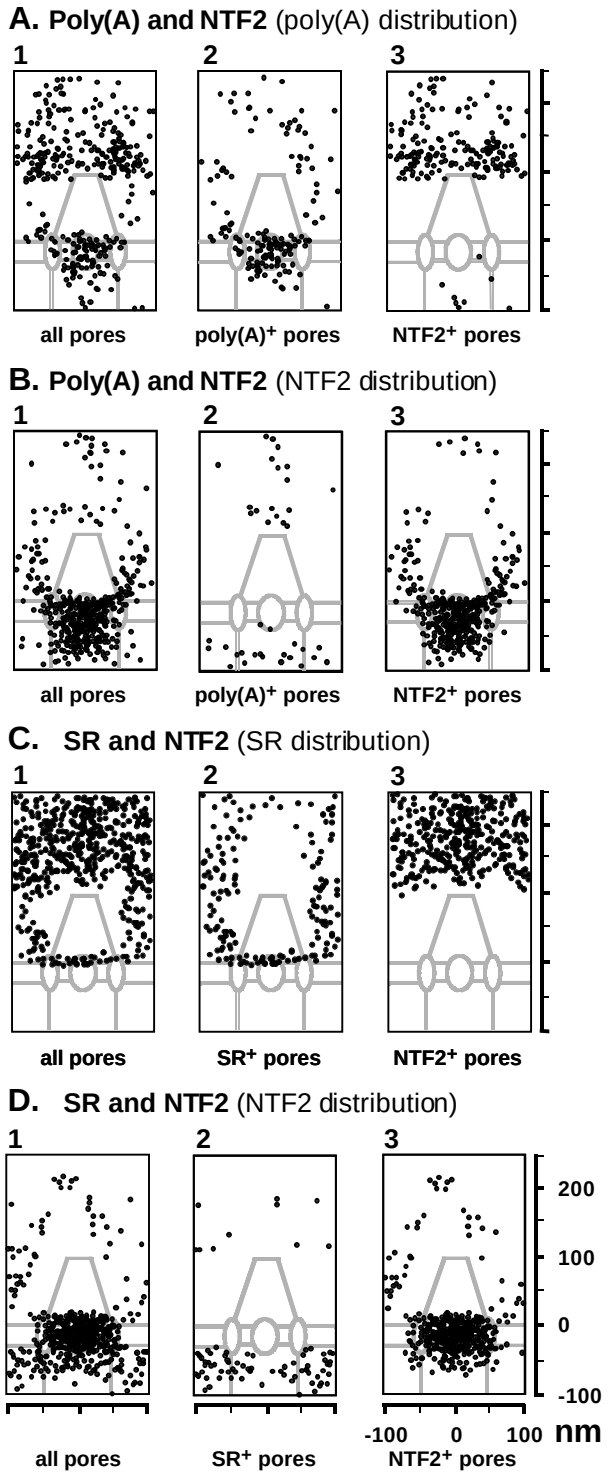

Fig. 6. Double-labelling shows that some pores in rat liver nuclei are associated with a particular marker to the exclusion of another. In each case, the complete distribution of a marker ('all pores' in column 1) was split into the two sub-populations indicated (columns 2 and 3). (A) The poly(A) distribution after double-labelling poly(A) and NTF2. Poly(A) is associated with 'poly(A)$^+$ pores', but only background levels are associated with 'NTF2$^+$ pores'. (B) The NTF2 distribution after double-labelling poly(A) and NTF2. The situation seen in A is reversed. (C) The SR distribution after double-labelling SR and NTF2. SR is associated with 'SR$^+$ pores', but not 'NTF2$^+$ pores'. (D) The NTF2 distribution after double-labelling SR and NTF2. The situation seen in C is reversed.

labelling (line 1), and 3.1% after double labelling (values added in lines 4 and 6). For NTF2, corresponding values were 34% (line 2) and 33.1% (values added in lines 5 and 6) or 34% (values added in lines 9 and 10). Moroever, under these conditions, there was no steric hindrance between probes directed against two markers that might be expected to be found together (i.e. the poly(A) and SR antigens associated with mRNA; Table 1, lines 12-15). Third, immunogold probes have diameters of ~20 nm, yet poly(A) and SR are still excluded from the much larger area of 'medium' size around 'NTF2$^+$ pores' (lines 6 and 10). Finally, no exclusion was seen between SR and NTF2 (and vice versa), or between poly(A) and NTF2 (and vice versa) in 8,000 randomly-selected squares (100 × 100 nm) in the interior of 20 different nuclei (not shown).

Phosphorus distributions determined by electron spectroscopic imaging

Electron spectroscopic imaging (ESI) can be used to map the distribution of phosphorus in cells (e.g. Hendzel and Bazett-Jones, 1996; Hendzel et al., 1998). An electron passing through the specimen can interact with a positively-charged atomic nucleus and be deflected from its path without energy loss. As the frequency of such elastic scattering increases with increasing atomic number, heavy elements like uranium, lead and osmium are used conventionally to enhance contrast (as in Fig. 2A). But the beam electron can also interact with a specimen electron and lose energy, and the loss in such inelastic scattering is characteristic of each element. Therefore, the energy-loss spectrum contains information on composition, making it possible to map the distribution of phosphorus-rich RNA in and around pores.

We calibrated the system using an established procedure and ribosomes essentially as described by Hendzel et al. (1998). Images of the same region of the cytoplasm were collected in different regions of the energy-loss spectrum; four are illustrated in Fig. 7A-D. The conventional (zero-energy loss) image reveals ribosomes strung along the endoplasmic reticulum (Fig. 7A), the second (-120 eV) reflects mass (Fig. 7B), the third (-155 eV) includes the contribution of phosphorus (Fig. 7C), and the fourth displays the net phosphorus distribution obtained by subtraction (Fig. 7D). This fourth image shows the RNA distribution, as phospholipids and highly-phosphorylated proteins contain so little phosphorus in comparison to the ~6,600 phosphorus atoms in rRNA. Thus, no phospholipid in membranes are detected in the 'net P' image (Fig. 7D), and even if every tenth amino acid in the ribosome were phosphorylated, <25% of the phosphorus would be in protein. However, ribosomes (diameters ~20 nm) have a range of intensities; although most lie completely within the ~40 nm section and so contain ~6,600 phosphorus atoms, many are cut randomly during sectioning and so lose mass and phosphorus, while a few lie above other ribosomes and can apparently contain up to twice the number of atoms (Hendzel et al., 1998). Therefore, experimentally-determined intensities can be related directly to absolute numbers of phosphorus atoms (Fig. 7, legend). The distribution seen (Fig. 7E, filled

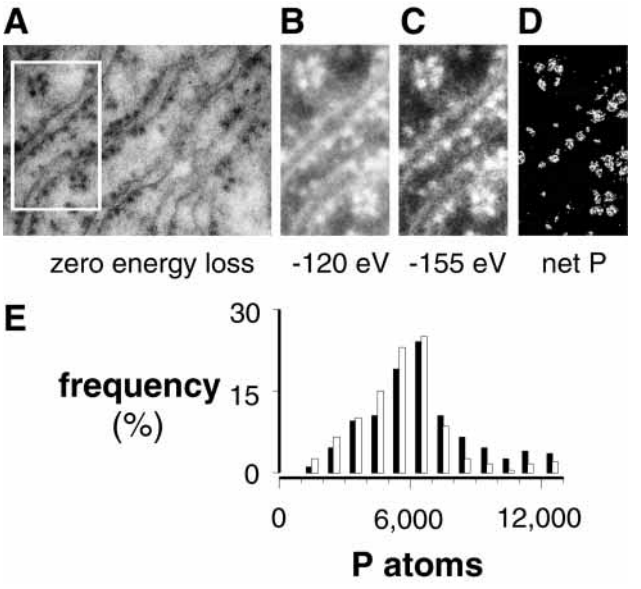

Fig. 7. Imaging phosphorus in ribosomes by ESI. (A) Conventional (zero-energy loss) image of electron-dense ribosomes associated with the endoplasmic reticulum. The region in the white rectangle is shown in B-D. (B) Image collected at −120 eV (whitest areas reflect highest mass). (C) Image collected at −155 eV which includes the contribution of phosphorus. (D) The net phosphorus distribution obtained by subtraction. Phosphorus-rich ribosomes appear white; they have a range of intensities because some lie on top of others, while others are cut randomly during sectioning and so lose a 'pole'. Bar, 100 nm. (E) Frequencies of ribosomes with different intensities. Intensities of 500 isolated ribosomes or ribosome pairs were measured in 10 images like that in D (filled rectangles) or in 10 simulated images of 40 nm sections of randomly-distributed spheres of 20 nm (open rectangles). Strings of >2 ribosomes apparently fused together are often seen associated with the endoplasmic reticulum (e.g. Fig. 8D) and were not counted. Summed intensities over the area occupied by each ribosome were related to the number of phosphorus atoms assuming that the most frequent class, which in both cases had the expected diameter of ~20 nm, contained 6,600 phosphorus atoms. The frequency distribution falls off above 6,600 atoms because few ribosomes lie on top of another in the section. No ribosomes with <600 atoms were seen in the real distribution.

rectangles) matched the distribution expected if the same numbers of ribosome-sized spheres had been sectioned randomly (Fig. 7E, open rectangles). This analysis also allows us to determine the threshold of detection. Some ribosomes would be expected to give 'polar caps' with so little phosphorus that they would go undetected; indeed, no ribosomes with <600 phosphorus atoms were seen (Fig. 7, legend). Therefore, we might expect to see at least a fraction of mRNA and rRNA (with ~1,500 and 6,600 phosphorus atoms, respectively) as it passed through the pores.

We next mapped the phosphorus distribution around 71 pores. Images of each pore were collected in different regions of the spectrum (e.g. Fig. 8A-C), and the net phosphorus image derived (e.g. Fig. 8D); then, the net phosphorus images were oriented in a stack, and the average intensity determined (Fig. 8F). (Fig. 8E shows the relative positions of pores within individual fields.) Phosphorus in heterochromatin generally frames each pore, but no membrane phospholipid is detected (Fig. 8A,D,F). However, about half the pores also contained some phosphorus in the gap in the membrane (e.g. Fig. 8D), which could be RNA in transit. Therefore, we subdivided pores into 'P^+ pores' and 'P^- pores' using the grey selection zone illustrated in Fig. 8E. (A smaller selection zone was used here because ESI gives higher resolution than immunolabelling.) Then, we examined the phosphorus distribution around the two kinds of pore, and found that they were different (Fig. 8G,H). We went on to obtain an image of the extra phosphorus associated with 'P^+ pores' by subtraction (Fig. 8I), and, again, this extra phosphorus could reflect the presence of RNA. Examination of these phosphorus distributions leads to several conclusions. First, no phosphorus is found in the centre of the basket (Fig. 8F), showing that this region around both types of pore contains little DNA or RNA. Second, if phosphorus marks RNA, then the RNA appears to enter the pore from the sides, perhaps to pass around the central transporter at the membrane (Fig. 8I). Third, pores can be categorized into two types; one contains phosphorus at the level of the membrane, the other does not (Fig. 8G,H). Fourth, many ribosomes are found in the cytoplasm immediately abutting 'P^+ pores', but not 'P^- pores' (Fig. 8I). Quantitative analysis confirmed this result. Thus, an average of 0.7±0.9 ribosomes were present in the grey zone in Fig. 8J abutting 'P^+ pores', while only 0.1±0.3 were found near 'P^- pores'; this difference was significant at the 0.9999 level (value calculated using 50 zero-energy loss images of each type, and Student's *t*-test; not shown). Ribosomes are also found along the outer membrane immediately next to 'P^+ pores', but not 'P^- pores' (Fig. 8I). Therefore, all these results are consistent with those obtained by immunolabelling. Even if the phosphorus seen is not in RNA, this data clearly shows that there are two distinct kinds of pore.

DISCUSSION

Paths through the pore

We investigated the path that RNA takes through nuclear pores using two methods. In one, HL60 cells were grown in Br-U so that the analogue is incorporated into RNA and exported to the cytoplasm. After embedding and cutting a section of ~50 nm, Br-RNA on one surface was immunolabelled with gold particles, and pores and associated particles imaged in the electron microscope. Such surface labelling over pores that have been sectioned equatorially provides better resolution than pre-embedment labelling, where particles are spread through the three-dimensions of the section. However, resolution is limited by the size of the probe (i.e. two immunoglobulins of ~9 nm and a gold particle of 5 or 10 nm), which is large relative to the structure being analyzed (in our case, a pore ~100 nm across). (Iborra and Cook (1998) evaluate the effects of probe size on resolution.) Moreover, precise quantization of different antigens is impossible, as they are detected with different efficiencies, and even the same one may be detected with different efficiencies in different sites. Nevertheless, this approach provides the highest resolution currently attainable by indirect immunogold labelling. We expected it to show that Br-RNA entered the pore complex through the tip of the basket, and to travel down the central axis to the transporter at the membrane (Fig. 9, left, route 1; Daneholt, 1997; Kiseleva et al., 1998). However, no Br-RNA

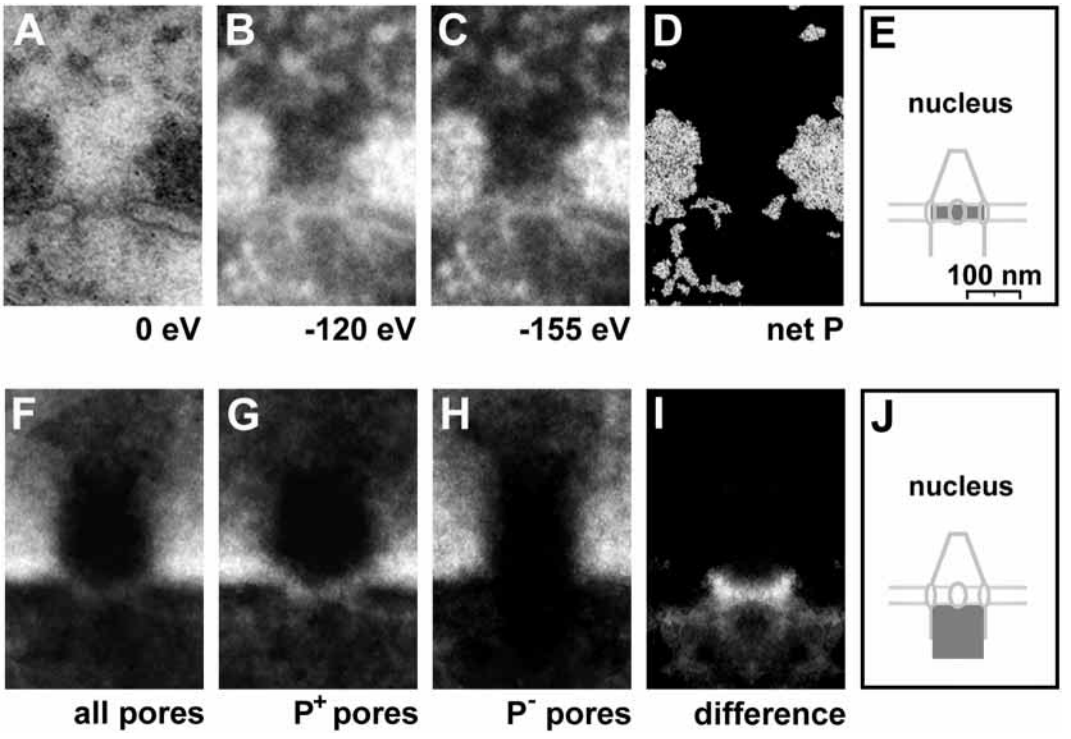

Fig. 8. The distribution of phosphorus in and around pores of rat liver nuclei determined by ESI. Pores are oriented within each field as indicated in E. (A) Conventional (zero-energy loss) image of a pore. (B) Image (reflecting mass) of the pore in A collected at –120 eV. (C) Image (which includes the contribution of phosphorus) of the pore in A collected at – 155 eV. (D) The net phosphorus distribution around the pore in A obtained by subtraction; this pore was categorized as 'phosphorus$^+$' (see E). (E) A cartoon of a pore; pores were categorized as 'phosphorus$^+$' if any phosphorus was detected in the grey selection zone of 100 × 30 nm. (F) The average phosphorus distribution obtained by stacking and orientating 71 randomly-selected images like that in D. (G) The average distribution around 50 'phosphorus$^+$' pores. (H) The average distribution around 50 'phosphorus$^-$' pores. (I) The difference in phosphorus signal obtained by subtracting intensity levels in H from those in G. (J) A cartoon of the pore and the selection zone (100 × 100 nm) used to confirm that more ribosomes were present next to 'P^+ pores' than 'P^- pores'.

was detected in the middle of the basket (i.e. in Fig. 9, left, zone b). Instead, it was distributed around the edges (Fig. 1), apparently entering from the sides close to the transporter (Fig. 9, left, route 2). As Br-RNA might not behave like its natural counterpart, we also localized various other markers in and around pores of rat liver nuclei, chosen because their pores are so easily identified in the native tissue (Fig. 2). Although some structural components of the pore (i.e. NUPs 62, 153, 250) were found along the central axis, other markers associated with mRNA (i.e. poly(A), hnRNPs A1 and C, mrnp 41, a subset of SR proteins, ASF) were all distributed at the periphery, as were some transport factors and their cargoes (i.e. NTF2, Ran, RCC1, karyopherin β, Rch1, transportin α, $m^{2,2,7}$-trimethylG; Fig. 3). These distributions strikingly resemble those of SV40 particles seen in infected nuclei, which are also excluded from the central axis (Maul, 1976).

Phosphorus, and so RNA, can be localized with even higher resolution by ESI (e.g. Hendzel and Bazett-Jones, 1996; Hendzel et al., 1998). The method proved sufficiently sensitive to detect ~600 phosphorus atoms in the RNA of a ribosome (Fig. 7); this is roughly two-fifths the number found in a typical message. Although a high background of phosphorus in DNA complicated analysis (e.g. Fig. 8A,D), no phosphorus was found in the centre of the basket (Fig. 8F,I). Therefore, the simplest interpretation of results obtained with the two different methods is that RNA is exported along route 2 through the left-hand pore in Fig. 9 (but see below). If proteins

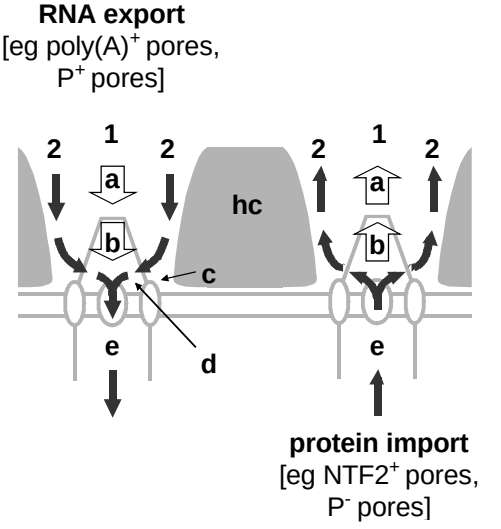

Fig. 9. Possible paths through dedicated pores. Left-hand pore. The current model sees messages travelling down route 1 to the transporter at the membrane. However, no Br-RNA, poly(A)$^+$ RNA, phosphorylated SR proteins, or phosphorus are seen in zone (b); instead, they are concentrated at the periphery, apparently on route 2. Zone (a): contains NTF2, but little pol(A)$^+$ RNA or phosphorylated SR proteins. Zone (b): contains no cargoes/factors. Zone (c): site where hnRNP C is removed. Zone (d): site where SR proteins are dephosphorylated. Zone (e): ribosome-rich. Right-hand pore. Various factors that usher proteins into the nucleus are found on route 2; they are never seen on route 1. Zone (a): contains 'poly(A)$^+$ RNA and phosphorylated SR proteins, but little NTF2. Zone (b): contains no cargoes/factors. Zone (e): ribosome-poor. hc: heterochromatin flanking pore.

on their way in are distributed like the shuttling protein, NTF2, they seem to follow the reverse path (Fig. 9, right, route 2).

The 75S RNA encoded by the BR genes of *Chironomus* seems to dock at the tip of the basket, before travelling down the central axis to the transporter (Fig. 9, left, route 1; Daneholt, 1997; Kiseleva et al., 1998). Moreover, in situ hybridization also shows poly(A)$^+$ RNA to be concentrated centrally (Huang et al., 1994). How can these observations be reconciled with ours? There are several possibilities. First, immunodetection in the central area might be poor, but then all cargoes/transport factors tested would have to be missed while all structural components were detected. The failure to detect any RNA in the central area by ESI also makes this possibility less likely. Second, cargoes/factors might travel so rapidly along route 1 that we miss them, and the concentration of markers along route 2 would then reflect stored cargoes/factors awaiting transport. In the absence of any kinetic data, it is difficult to eliminate this possibility; however, given the range of cargoes/factors tested and the use of two independent methods, it is striking that none were ever seen on route 1 near the tens of thousands of pores analyzed. Third, perhaps cargoes do follow route 2, and then the convincing work on *Chironomus* could be re-interpreted as follows. Although baskets have been seen using a range of techniques, these techniques have all been applied to isolated nuclear membranes. However, with unextracted material, filaments (but not baskets) are seen extending from pores into the nuclear interior (e.g. Richardson et al., 1988; Arlucea et al., 1998). Indeed, Arlucea et al. (1998) have suggested that these filaments are necessarily severed when nuclear membranes are isolated, and that they collapse inwards to create the structures commonly called 'baskets'. Then, any RNA attached to these peripheral filaments would also collapse into the centre on isolation, and so would appear to be part of the 'basket'. The axial location of poly(A)$^+$ RNA seen by Huang et al. (1994) would then reflect differences in technique and resolution; they detected a hybridized probe using immunoperoxidase, and, under the conditions used, the resulting precipitate could easily have diffused into the central region (e.g. Courtoy et al., 1983). Whatever the true explanation, we hope that our results will prompt a reinvestigation of the pathway using high resolution techniques, natural cargoes, and intact cells.

Different classes of pore

Blobel (1985) originally suggested that particular pores might become dedicated to the import or export of particular cargoes; one pore might export cargo A, while another imported cargo B. Therefore we applied both methods to see whether pores associate with different markers. For this analysis, we need make no assumptions as to whether the chosen marker is exported or imported; we are initially concerned with whether a pore associates with one of two markers, or both. We found that pores with poly(A) in the gap in the membrane had no NTF2 for 100 nm into the nucleus, and those with NTF2 had no poly(A) (Fig. 6A,B). Similarly, phosphorylated SR proteins were completely excluded from a zone around 'NTF2$^+$ pores' (Fig. 6C,3), and vice versa (Fig. 6C,D). Moreover, some pores contained phosphorus in the gap while others did not; ribosomes often lay close to the 'phosphorus$^+$ pores' (both in the cytoplasm and along the outer nuclear membrane), while being excluded from this zone near 'phosphorus$^-$ pores' (Fig. 8F-I). Clearly, each of these different markers associates with particular pores. Given such specialization, it is easy to imagine that flux across the membrane would be facilitated by dedicating (at any one moment) whole pores to export or import (Fig. 9).

Such dedication raises many questions. First, how can our results be reconciled with others suggesting that pores are bifunctional? Thus, when gold particles coated with mRNA (or nuclear localization signals) are introduced into the nucleus (or cytoplasm) of oocytes, they soon associate with most pores (Dworetzky and Feldherr, 1988; Newmeyer and Forbes, 1988); this implies that all pores export/import simultaneously. Moreover, coinjections reveal gold particles apparently entering and exiting through the same pores (Dworetzky and Feldherr, 1988). However, these experiments involve unatural substrates introduced in excess; they could easily saturate the system and reverse flow through previously-dedicated pores (Nakielny et al., 1997). Alternatively, oocytes might not contain differentiated pores like rat liver nuclei. Second, what fraction of pores might be involved in exporting messages? We find 3% pores associated with poly(A)$^+$ RNA at the level of the membrane (Table 1, line 1, 'small' field), and, as our detection methods are not one-hundred percent efficient, this would represent a minimum. By the same reasoning, ≥50% might be involved in export of RNA of all types (Fig. 8), and ≥34% pores in NTF2-mediated transport (Table 1, line 2, 'small' field). Third, how might the whole of a pore associate with one marker to the exclusion of another? Consider two undifferentiated pores. We might imagine that once NTF2 had facilitated import through one pore, it would be more likely to recycle back through the same pore; if more NTF2 then bound cooperatively, it might soon line the whole pore. If the second pore happened to export a message first, recycling its transport factor would locally concentrate that factor, and cooperative binding would generate a message-exporting pore. Then, the pressure of mass action could reverse polarity when the concentration of a natural cargo/factor (or mRNA-gold in the microinjection experiments discussed above) reached a critical concentration. Fourth, if pores so change from one type to another, how quickly might they do so? As ribosomes probably redistribute slowly in the cytoplasm, it seems likely that 'phosphorus$^+$ pores' will also convert slowly into 'phosphorus$^-$ pores'. However, the answers to all these questions must await further analysis. But whatever the explanation, we have found different classes of pores associated with specialized zones on both sides of the membrane (Fig. 9).

We thank the Wellcome Trust and Cancer Research Campaign for support, G. Blobel, G. Dreyfuss, A. Krainer, M. Lloyd and J. Renau-Piqueras for kindly supplying antibodies or software, and J. Sanderson and J. Bartlett for their help.

REFERENCES

Akey, C. W. and Radermacher, M. (1993). Architecture of the Xenopus nuclear pore complex revealed by three-dimensional cryo-electron microscopy. *J. Cell Biol.* **122**, 1–19.

Akey, C. W. (1995). Structural plasticity of the nuclear pore complex. *J. Mol. Biol.* **248**, 273-293.

Arlucea, J., Andrade, R., Alonso, R. and Aréchaga, J. (1998). The nuclear basket of the nuclear pore complex is part of a higher-order filamentous network that is related to chromatin. *J. Struct. Biol.* **124**, 51-58.

Bangs, P., Burke, B., Powers, C., Craig, R., Purohit, A. and Doxsy, S. (1998). Functional analysis of Tpr: identification of nuclear pore complex association and nuclear localization domains and a role in mRNA export. *J. Cell Biol*. **143**, 1801-1812.

Bastos, R., Panté, N. and Burke, B. (1995). Nuclear pore complex proteins. *Int. Rev. Cytol*. **162B**, 257-302.

Blobel, G. (1985). Gene gating: a hypothesis. *Proc. Nat. Acad. Sci. USA* **82**, 8527–8529.

Bozzola, J. J. and Russell, L. D. (1992). *Electron Microscopy: Principles and Techniques for Biologists*. Jones and Bartlett, Boston.

Cáceres, J. F., Screaton, G. R. and Krainer, A. R. (1998). A specific subset of SR proteins shuttles continuously between the nucleus and the cytoplasm. *Genes Dev*. **12**, 55-66.

Cordes, V. C., Reidenbach, S., Rackwitz, H. R. and Franke, W. W. (1997). Identification of protein p270/Tpr as a constitutive component of the nuclear pore complex-attached intranuclear filaments. *J. Cell Biol*. **136**, 515-529.

Courtoy, P. J., Picton, D. H. and Farquhar, M. G. (1983). Resolution and limitations of the immunoperoxidase procedure in the localization of extracellular matrix antigens. *J. Histochem. Cytochem*. **31**, 945-951.

Daneholt, B. (1997). A look at messenger RNP moving through the nuclear pore. *Cell* **88**, 585-588.

Davis, L. I. and Blobel, G. (1986). Identification and chraracterization of a nuclear pore complex protein. *Cell* **45**, 699-709.

Dworetzky, S. I. and Feldherr, C. M. (1988). Translocation of RNA-coated gold particles through the nuclear pores of oocytes. *J. Cell Biol*. **106**, 575-584.

Feldherr, C. M. and Akin, D. (1997). The location of the transport gate in the nuclear pore complex. (1997). *J. Cell Sci*. **110**, 3065-3070.

Franke, W. W. and Scheer, U. (1974). Structures and functions of the nuclear envelope. *Cell Nucleus* **1**, 219-347.

Goldberg, M. W. and Allen, T. D. (1992). High resolution scanning electron microscopy of the nuclear envelope: demonstration of a new, regular, fibrous lattice attached to the baskets of the nucleoplasmic face of the nuclear pores. *J. Cell Biol*. **119**, 1429-1440.

Görlich D. and Mattaj, I. W. (1996). Nucleocytoplasmic transport. *Science* **271**, 1513–1518.

Görlich, D., Pante, N., Kutay, U., Aebi, U. and Bischoff, F. R. (1996). Identification of different roles for RanGDP and RanGTP in nuclear protein import. *EMBO J.* **15**, 5584-5594.

Griffiths, G. (1993). *Fine Structure Immunocytochemistry*. Springer-Verlag, Berlin, Heidelberg. 459 pp.

Hendzel, M. J. and Bazett-Jones, D. P. (1996). Probing nuclear ultrastructure by electron spectroscopic imaging. *J. Microsc.* **182**, 1-14.

Hendzel, M. J., Kruhlak, M. J. and Bazett-Jones, D. P. (1998). Organization of highly acetylated chromatin around sites of heterogeneous nuclear RNA accumulation. *Mol. Biol. Cell* **9**, 2491-2507.

Huang, S., Deerinck, T. J., Ellisman, M. H. and Spector, D. L. (1994). In vivo analysis of the stability and transport of nuclear poly(A)+ RNA. *J. Cell Biol*. **126**, 877-899.

Iborra, F. J., Pombo, A., Jackson, D. A. and Cook, P. R. (1996). Active RNA polymerases are localized within discrete transcription 'factories' in human nuclei. *J. Cell Sci*. **109**, 1427-1436.

Iborra, F. J. and Cook, P. R. (1998). The size of sites containing SR proteins in human nuclei: problems associated with characterizing small structures by immunogold labelling. *J. Histochem. Cytochem*. **46**, 985-992.

Iborra, F. J., Jackson, D. A. and Cook, P. R. (1998). The path of transcripts from extra–nucleolar synthetic sites to nuclear pores: transcripts in transit are concentrated in discrete structures containing SR proteins. *J. Cell Sci*. **111**, 2269-2282.

Jarnik, M. and Aebi, U. J. (1991). Toward a more complete 3-D structure of the nuclear pore complex. *Struct. Biol*. **107**, 291-308.

Kiseleva, E., Goldberg, M. W., Allen, T. D. and Akey, C. W. (1998). Active nuclear pore complexes in *Chironomus*: visualization of transporter configurations related to mRNP export. *J. Cell Sci*. **111**, 223-236.

Koepp, D. M. and Silver, P. A. (1996). A GTPase controlling nuclear trafficking: running the right way or walking RANdomly? *Cell* **87**, 1-4.

Kraemer, D. and Blobel, G. (1997). mRNA binding protein mrnp 41 localizes to both nucleus and cytoplasm. *Proc. Nat. Acad. Sci. USA* **94**, 9119-9124.

Mattaj, I. W. and Englmeier, L. (1998). Nucleocytoplasmic transport. *Annu. Rev. Biochem*. **67**, 265-306.

Maul, G. G. (1976). Fibrils attached to the nuclear pore prevent egress of SV40 particles from the infected nucleus. *J. Cell Biol*. **70**, 714-719.

Melchior, F., Paschal, B., Evans, J. and Gerace, L. (1993). Inhibition of nuclear protein import by nonhydrolyzable analogues of GTP and identification of the small GTPase Ran/TC4 as an essential transport factor. *J. Cell Biol*. **123**, 1649-1659.

Moore, M. S. and Blobel, G. (1994). Purification of a Ran-interacting protein that is required for protein import into the nucleus. *Proc. Nat. Acad. Sci. USA* **91**, 10212-10216.

Moroianu, J., Hijikata, M., Blobel, G. and Radu, A. (1995). Mammalian karyopherin alpha 1 beta and alpha 2 beta heterodimers: alpha 1 or alpha 2 subunit binds nuclear localization signal and beta subunit interacts with peptide repeat-containing nucleoporins. *Proc. Nat. Acad. Sci. USA* **92**, 6532-6536.

Nakielny, S. and Dreyfuss, G. (1997). Nuclear export of proteins and RNAs. *Curr. Opin. Cell Biol*. **9**, 420-429.

Nakielny, S., Fischer, U., Michael, W. M. and Dreyfuss, G. (1997). RNA transport. *Annu. Rev. Neurosci*. **20**, 269-301.

Newmeyer, D. D. and Forbes, D. J. (1988). Nuclear import can be separated into distinct steps in vitro: nuclear pore binding and translocation. *Cell* **52**, 641-653.

Nigg, E. A. (1997). Nucleocytoplasmic transport: signals, mechanisms and regulation. *Nature* **386**, 779-787.

Panté, N., Bastos, R., McMorrow, I., Burke, B. and Aebi, U. (1994). Interactions and three dimensional localization of a group of nuclear pore complex proteins. *J. Cell Biol*. **126**, 603-617.

Panté, N. and Aebi, U. (1996). Molecular dissection of the nuclear pore complex. *Crit. Rev. Biochem. Mol. Biol*. **31**, 153-199.

Panté, N., Jarmolowski, A., Izaurralde E., Sauder, U., Baschong, W. and Mattaj, I. W. (1997). Visualizing nuclear export of different classes of RNA by electron microscopy. *RNA* **3**, 498-513.

Paschal, B. M. and Gerace, L. (1995). Identification of NTF2, a cytosolic factor for nuclear import that interacts with nuclear pore complex protein p62. *J. Cell Biol*. **129**, 925-937.

Piñol-Roma, S. and Dreyfuss, G. (1992). Shuttling of pre-mRNA binding proteins between nucleus and cytoplasm. *Nature* **355**, 730-732.

Pollard, V. W., Michael, W. M., Nakielny, S., Siomi, M. C., Wang, F. and Dreyfuss, G. (1996). A novel receptor-mediated nuclear protein import pathway. *Cell* **86**, 985-994.

Renau-Piqueras, J., Renau-Piqueras, J., Zaragoza, R., De-Paz, P., Baguena-Cervellera, R., Megias, L. and Guerri, C. (1989). Effects of prolonged ethanol exposure on the glial fibrillary acidic protein-containing intermediate filaments of astrocytes in primary culture: a quantitative immunofluorescence and immunogold electron microscopic study. *J. Histochem. Cytochem*. **37**, 229-240.

Rexach, M. and Blobel, G. (1995). Protein import into nuclei: association and dissociation reactions involving transport substrate, transport factors, and nucleoporins. *Cell* **83**, 683-692.

Richardson, W. D., Mills, A. D., Dilworth, S. M., Laskey, R. A. and Dingwall, C. (1988). Nuclear protein migration involves two steps: rapid binding at the nuclear envelope followed by slower translocation through nuclear pores. *Cell* **52**, 655-664.

Roth, M. B., Zahler, A. M. and Gall, J. G. (1990). A monoclonal antibody that recognizes a phosphorylated epitope stains lampbrush chromosomes and small granules in the amphibian germinal vesicle. *J. Cell Biol*. **111**, 2217-2223.

Smith, A., Brownawell, A. and Macara, I. G. (1998). Nuclear import of Ran is mediated by the transport factor NTF2. *Curr. Biol*. **8**, 1403-1406.

Stevens, B. J. and Swift, H. (1966). RNA transport from nucleus to cytoplasm in Chironomus salivary glands. *J. Cell Biol*. **31**, 55-77.

Ullman, K. S. Powers, M. A. and Forbes, D. J. (1997). Nuclear export receptors: from importin to exportin. *Cell* **90**, 967-970.

Visa, N., Puvion-Dutilleul, F., Harper, F., Bachellerie, J. P. and Puvion, E. (1993). Intranuclear distribution of poly(A) RNA determined by electron microscope in situ hybridization. *Exp. Cell Res*. **208**, 19-34.

Yang, Q., Rout, M. P. and Akey, C. W. (1998). Three-dimensional architecture of the isolated yeast nuclear pore complex: functional and evolutionary implications. *Mol. Cell* **1**, 223-234.

Zahler, A. M., Lane, W. S., Stolk, J. A. and Roth, M. B. (1992). SR proteins: a conserved family of pre-mRNA splicing factors. *Genes Dev*. **6**, 837-847.